energies

MDPI

Article

Solar Energy Driven Membrane Desalination: Experimental Heat Transfer Analysis

Hosam Faqeha [1,2,*], Mohammed Bawahab [2,3], Quoc Linh Ve [2,4], Oranit Traisak [2], Ravi Koirala [2], Aliakbar Akbarzadeh [2] and Abhijit Date [2,*]

[1] Mechanical Engineering Department, College of Engineering and Islamic Architecture, Umm Al-Qura University, P.O. Box 715, Makkah 21955, Saudi Arabia
[2] Mechanical and Automotive Engineering, School of Engineering, RMIT University, Bundoora, VIC 3083, Australia
[3] Department of Mechanical Engineering, Faculty of Engineering, University of Jeddah, Jeddah 23890, Saudi Arabia
[4] Faculty of Engineering and Food Technology, University of Agriculture and Forestry, Hue University, Hue 530000, Thua Thien Hue, Vietnam
* Correspondence: hzfaqeha@uqu.edu.sa (H.F.); abhijit.date@rmit.edu.au (A.D.)

Abstract: In the direct contact membrane distillation (DCMD) system, the temperature polarization due to boundary layer formation limits the system performance. This study presents the experimental results and heat transfer analysis of a DCMD module coupled with a salinity gradient solar pond (SGSP) under three different flow channel configurations. In the first case, the feed and permeate channels were both empty, while in the next two cases, the feed and permeate channels were filled with a porous spacer material. Two different spacer geometries are examined: 1.5 mm thick with a filament angle of 65°, and 2 mm thick with a filament angle of 90°. The study considers only the heat transfer due to conduction by replacing the hydrophobic membrane normally used in a DCMD module with a thin polypropylene sheet so that no mass transfer can occur between the feed and permeate channels. The Reynolds number for all three configurations was found to be between 1000 and 2000, indicating the flow regime was laminar. The flow rate through both the feed and permeate sides was the same, and experiments were conducted for flow rates of 5 L/min and 3 L/min. It has been found that the highest overall heat transfer coefficient was obtained with the spacer of 2 mm thickness and filament angle of 90°.

Keywords: water desalination; membrane desalination; solar pond; heat transfer

check for updates

Citation: Faqeha, H.; Bawahab, M.; Linh Ve, Q.; Traisak, O.; Koirala, R.; Akbarzadeh, A.; Date, A. Solar Energy Driven Membrane Desalination: Experimental Heat Transfer Analysis. *Energies* **2022**, *15*, 8051. https://doi.org/10.3390/en15218051

Academic Editor: Alessandra Criscuoli

Received: 15 October 2022
Accepted: 25 October 2022
Published: 29 October 2022

Publisher's Note: MDPI stays neutral with regard to jurisdictional claims in published maps and institutional affiliations.

Copyright: © 2022 by the authors. Licensee MDPI, Basel, Switzerland. This article is an open access article distributed under the terms and conditions of the Creative Commons Attribution (CC BY) license (https://creativecommons.org/licenses/by/4.0/).

1. Introduction

Water is a common, widely available substance. However, only about 3% of it is available for human consumption. The remaining 97% is seawater. The availability of even this 3% is affected by various factors. Environmental pollution is one problem. According to the World Health Organization (WHO) and the United Nations International Children's Emergency Fund (UNICEF), about 2.1 billion people are deprived of access to safe, readily available water at home and about 4.5 billion people do not have safe sanitation facilities [1]. The problem is severe in the rural and remotely located areas of developing countries. Although access to water has increased over the years, access to safe water and sanitation is still a severe problem. The global population was 7.66 billion in November 2018 and is expected to reach 8.5 billion by 2030 and 9.7 billion by 2050 [2]. It has been increasing rapidly since the industrial revolution of the 1800s, growing from 1.65 billion to 6 billion during the 20th century. However, it is expected to take about 200 years for the current population to double, compared to the 58 years it took to double from three billion to six billion. However, the population is expected to increase at a much higher rate in certain regions such as the Middle East and Sub-Saharan Africa, South Asia,

Southeast Asia, and Latin America. Such growing population density in certain areas can lead to heavy water demand combined with more significant pollution problems.

Traditional water treatment methods such as multistage flash (MSF), multi effect distillation (MED), and reverse osmosis (RO) need either high temperature thermal energy or electrical energy for operation. On the other hand, membrane desalination can operate at much lower temperatures and hence in recent years there has been a significant research focus on the development of membrane desalination systems. In this process, a microporous hydrophobic membrane is used to separate liquids from dissolved solids [3]. The general types of MD system configurations listed below are shown in Figure 1:

- direct contact membrane distillation (DCMD);
- sweep gas membrane distillation (SGMD);
- vacuum membrane distillation (VMD);
- air gap membrane distillation (AGMD).

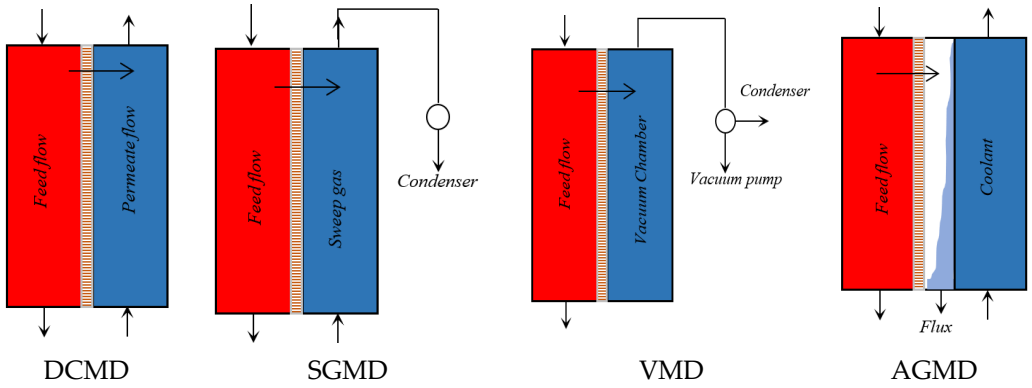


Figure 1. Schematic of different types of membrane desalination systems.

In DCMD, the feed solution is heated and is in direct contact with the surface of the membrane. Therefore, quick evaporation occurs at the feedwater–membrane interface. Vapor moves across the membrane due to the vapor pressure difference and then condenses inside the membrane module. The hydrophobic nature of the membrane prevents the liquid feedwater from penetrating the membrane, hence, vapor can only exist inside the membrane pores. The DCMD configuration is the most straightforward configuration of membrane distillation technologies. Hence, there is more widespread use of DCMD compared to these other configurations. The heat lost by conduction is a significant limitation of DCMD. Although the thermal conductivity of polymeric membranes is typically minimal, the driving force for the desalination, i.e., the temperature differential, results in considerable conductive heat transfer through the membrane material due to its minimal thickness. As a result, DCMD has the highest energy loss by thermal conduction of any MD configuration, resulting in low thermal efficiency [4]. DCMD is used in a variety of industrial applications, including the desalination and concentration of aqueous solutions in food industries and the manufacture of acids [5,6].

DCMD can be used for desalination and concentration of aqueous solutions; however low energy efficiency is a major drawback affecting its use in large-scale applications. The mass flux and energy efficiency can be increased by reducing the temperature polarization. The first step for this is to understand the effects of flow regime on the heat transfer in the absence of mass transfer. Hence, the estimation of heat transfer coefficients is essential for analysis and design of efficient MD modules. Some recent research work on these aspects is reviewed below.

An early study on the use of spacer-filled channels in MD applications by Martınez-Dıez, Vázquez-González, and Florido-Dıaz [7] showed advantages in terms of enhanced heat and mass transfers using low-grade heat sources. In commercially available membrane distillation modules, the feed and permeate flow channels have different spacer material and orientation. In a numerical study, Taamneh [8] found that the spacer increased shear

stress at the wall and doubled the Nusselt number in contrast to an empty channel. In a DCMD module, mass flux enhancement by spacers was detected by Phattaranawik, Jiraratananon, Fane, and Halim [9]. The authors developed a model to explain mass flux increases due to spacers. Phattaranawik et al. [10] tested net type spacers fitted in DCMD to enhance mass transfer coefficient. In their work, Yun, Wang, Ma, and Fane [11] studied the effects of spacers on flux enhancement of DCMD using a high concentration NaCl aqueous solution. The observed increase in mass flux was highest for the thick spacer, then thin spacer, and then without spacer. Taamneh and Bataineh [12] used experimental and numerical methods to test the effect of presence and orientation of filaments in spacers. An empty channel was used for comparison.

A study on the trans-membrane heat and mass transfer using comprehensive 3D CFD simulation covering the entire length of the module done by Chang, Hsu, Chang, and Ho [13] showed that spacers created high velocity regions near the membrane surfaces. The reputation in spacer geometry results in irregularity in heat and mass flux.

Gong et al. [14] proposed a new design with solar energy and graphene membrane, called solar vapor gap membrane distillation (SVGMD). They showed that this design has high energy efficiency and long-term stability and anti-fouling properties.

Quoc Linh Ve et al. [15] performed experimental analysis to determine the coefficient of heat and mass transfer for DCMD. The experiment used copper plate for different conditions; empty and spacer filled. The heat transfer correlations were within an acceptable limit.

In a different application of MD, AGMD, Chernyshov, Meindersma, and De Haan [7] investigated five geometries with the same thickness and different geometry. With spacers, about 2.5 times higher flux was noted when compared with an empty channel, in another application of MD

This seems to be higher than noted for DCMD. Different types of spacer configurations were determined to be optimum depending on the different levels of importance attached to either temperature or mass fluxes.

The objective of this experimental work is to determine the overall heat transfer coefficient of a DCMD module with and without a spacer-filled channel to help understand the effects of spacer on the temperature polarization. The channel gap of the DCMD module was fixed, and the tests were conducted for three different configurations; empty channel, thin spacer-filled channel, and thick spacer filled channel and compared with heat transfer correlations presented in the literature to find the best fit.

2. Theory on Heat Transfer Phenomena in DCMD

Complex transport processes, including mass and heat transfer, occur concurrently throughout the DCMD process as seen in Figure 2. A DCMD module is typically composed of a flat module which has a feed chamber (for hot feedwater) and a cooling permeate chamber separated by a hydrophobic microporous membrane. Heat transfer occurs via convection/conduction across membrane (from feed to permeate) and convection/mass transfer (vapor transport) through the membrane pores.

On the feed side, the feedwater temperature (T_f) drops from the bulk fluid temperature to the membrane surface temperature (T_{mf}) across the boundary layer. As the vapor from the feed side condenses in the water on the permeate side, the permeate stream temperature increases. This results in a decreasing temperature gradient between the permeate fluid nearest the membrane (T_{mp}), through the boundary layer to the bulk fluid stream (T_p). The driving force is the difference in vapor pressure resulting from the difference in the interface temperatures on the feed and permeate sides (T_{mf} and T_{mp}). This is lower than the difference between bulk feed and permeate temperatures (T_f and T_p).

The temperatures near the membrane surfaces vary from the bulk fluid temperatures due to the heat transfer that occurs throughout the DCMD process. This results in the reduction in the driving force, and hence mass flux, compared to what would be expected based on the bulk fluid temperatures. This "is known as temperature polarization and the

temperature polarization coefficient (*TPC*) is the ratio between the actual driving force and the theoretical driving force" [16–18].

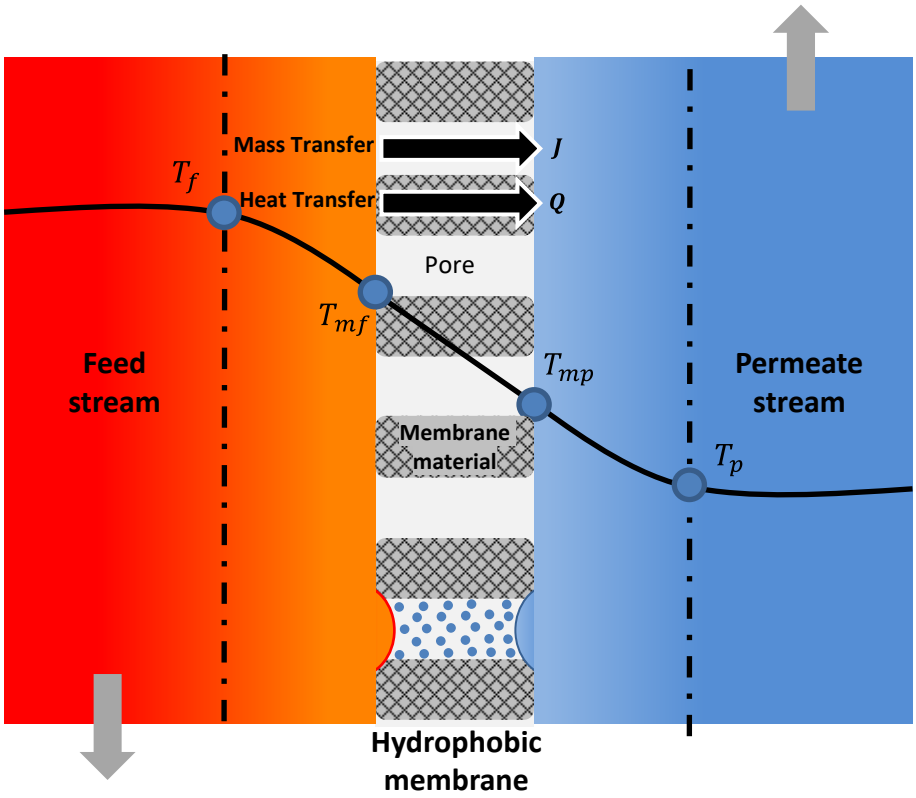


Figure 2. Schematic diagram of the transport mechanism for the direct contact membrane distillation (DCMD) process.

The Laplace–Young equation describes the pressure differential between liquid–vapor interfaces. The liquid entry pressure (*LEP*) of a membrane is defined as the lowest possible value of the hydrostatic pressure difference at which the feed liquid may pass through the biggest holes of the membrane. The interfacial tension, the liquid's contact angle at the pore entrance, and the size and shape of membrane pores all have a role in the liquid entry pressure. Franken et al. proposed the simple approach for determining the *LEP* value using the Laplace–Young equation [19].

Although they are not specifically mentioned, the operating temperature and the composition of the process solution may have a considerable effect on the liquid–solid contact angle and liquid surface tension. Therefore, when choosing a membrane, these impacts should not be ignored.

PTFE, PP, and polyvinylidene fluoride (PVDF) are the most often utilized materials for MD membranes. MD membrane porosity has been observed to vary between 35% and 93%, pore size typically varies between 100 nm and 1 µm, and membrane thickness typically s between 0.04 and 0.25 mm [20].

2.1. Mechanism of Heat Tramsfer

Heat transfer in the proposed module configuration with impermeable membrane occurs in three regions, defined in Figure 3. Heat transfer by convection occurs on the feed side from the fluid to the membrane; heat is then transferred by conduction through the thin plastic sheet; and finally, heat transfer by convection occurs on the permeate side from the membrane to the fluid. It should be noted that heat transfer resulting from the mass transfer would also occur if a vapor-permeable membrane was used. Figure 3 depicts the heat transfer thermal resistance model used in this study.

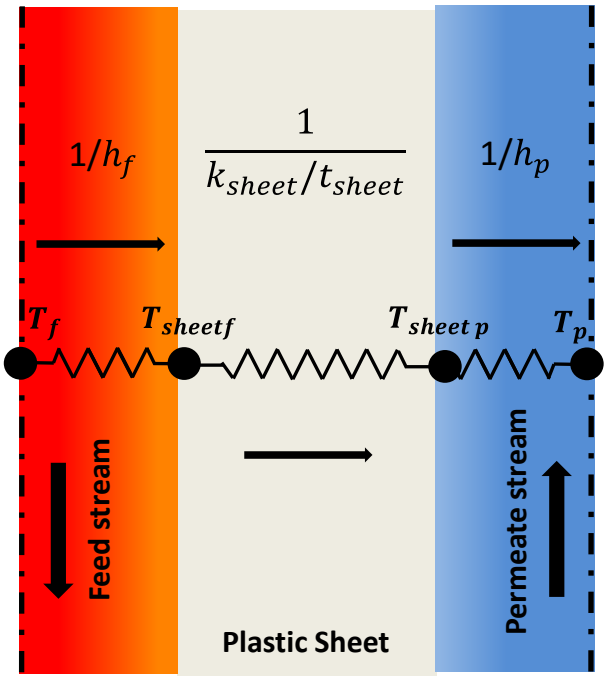


Figure 3. The thermal resistance series in empty and spacer-filled channels.

Equations (1) and (2) give convective heat transfer across feed to permeate side [21]:

$$\dot{Q}_f = \dot{m} \times C_p \times \left(T_{f,in} - T_{f,out}\right) \quad (1)$$

$$\dot{Q}_p = \dot{m} \times C_p \times \left(T_{p,out} - T_{p,in}\right) \quad (2)$$

$$\dot{Q}_f = h_f \times A_m \times \left(T_f - T_{sheet,f}\right) \quad (3)$$

$$\dot{Q}_p = h_p \times A_m \times \left(T_{sheet,p} - T_p\right) \quad (4)$$

where the difference between $T_{sheet,f}$ and $T_{sheet,p}$ is assumed to be negligible due to the small thickness of the plastic sheet (0.1 mm).

Here T_f and T_p; are the average bulk temperature of fluid for both sides. It is calculated using Equations (5) and (6)

$$T_f = \frac{T_{f,in} + T_{f,out}}{2} \quad (5)$$

$$T_p = \frac{T_{p,out} + T_{p,in}}{2} \quad (6)$$

The following Equation (7) can be used to determine the overall heat transfer coefficient of the DCMD module:

$$U = \left[\frac{1}{h_f} + \frac{t_{sheet}}{k_{sheet}} + \frac{1}{h_p}\right]^{-1} \quad (7)$$

2.2. Empty Channel

For the case where an empty channel is used, the experiments were conducted using the DCMD configuration module. The heat transfer coefficients are assumed to equal the same mass flow rate for both feed and permeate sides, and channel geometry was used. The Nusselt number for the experiments can be found in Equation (8)

$$Nu_{exp} = \frac{h * D}{k} \quad (8)$$

where $h = h_f = h_p$, and k and D are thermal conductivity and hydraulic diameter, respectively. Hydraulic diameter D can be determined by

$$D = \frac{2 * W * t}{W + t} \tag{9}$$

Table 1 shows different heat transfer correlations suggested in the literature. In order to determine the optimal heat transfer correlation for the DCMD configurations considered here, these correlations are used to determine a theoretical Nusselt number. These are then compared to the Nusselt numbers obtained from the experiments discussed in Sections 3 and 4. The best correlation is based on the minimum variation between experimental and theoretical Nusselt numbers, for a given configuration. The Reynolds number and Prandtl number required for the correlations in Table 1 can be estimated using the following equations.

Table 1. Different types of heat transfer correlation with Reynolds number in laminar flow range.

Correlation	Equation Number	Reference
$Nu = 1.86 \left(\frac{Re\ Pr}{L/D} \right)^{\frac{1}{3}}$	(10)	[22]
$Nu = 1.95 \left(\frac{Re\ Pr}{L/D} \right)^{\frac{1}{3}}$	(11)	[23]
$Nu = 4.36 + \frac{0.036 Re\ Pr(D/L)}{1 + 0.0011(Re\ Pr(D/L))^{0.8}}$	(12)	[21]
$Nu_{cooling} = 11.5(Re\ Pr)^{0.23}(D/L)^{0.5}$, $Nu_{heating} = 15(Re\ Pr)^{0.23}(D/L)^{0.5}$	(13)	[24]
$Nu = 0.13 Re^{0.64} Pr^{0.38}$	(14)	[24]
$Nu = 0.097 Re^{73} Pr^{0.13}$	(15)	[25]
$Nu = 3.66 + \frac{0.104 Re\ Pr(D/L)}{1 + 0.0106(Re\ Pr(D/L))^{0.8}}$	(16)	[23]
$Nu = 4.86 + \frac{0.06063(Re\ Pr(D/L))^{1/2}}{1 + 0.09094(Re\ Pr(D/L))^{0.7}\ Pr^{0.17}}$	(17)	[26]
$Nu = 1.62 \left(\frac{Re\ Pr}{L/D} \right)^{0.33}$	(18)	[21]

$$Re = \frac{\rho * u * D}{\mu} \tag{19}$$

$$Pr = \frac{\mu * C_p}{k} \tag{20}$$

where u is the superficial velocity of the fluid flow and can be determined by,

$$u = \frac{V}{W * t} \tag{21}$$

the overall heat transfer coefficient can be determined from the experimental results using Equations (22) and (23) as suggested by Ve and Rahaoui [15].

$$U = \frac{\dot{Q}}{A * \Delta T_{LMTD}} \tag{22}$$

where:

$$\Delta T_{LMTD} = \frac{\left(T_{f,in} - T_{p,out}\right) - \left(T_{f,out} - T_{p,in}\right)}{ln\left[\left(T_{f,in} - T_{p,out}\right) / \left(T_{f,out} - T_{p,in}\right)\right]} \quad (23)$$

2.3. Spacer-Filled Condition

The net-type spaces are common in membrane modules for commercial systems (ultrafiltration/spiral wound reverse osmosis). They can provide structural support to the membrane and, depending on the orientation of the spacer, can also cause the fluid flow to transition from a laminar to a localized turbulent flow regime. In a DCMD module, turbulent flow improves heat transfer. This increases the driving temperature difference, and hence the production of freshwater, and decreases the effect of temperature polarization. The spacer orientation, geometry, and its relation to the flow direction are illustrated in Figure 4.

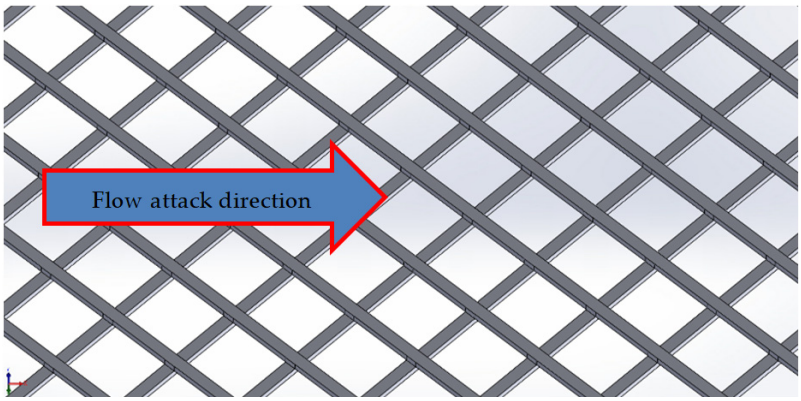


Figure 4. Spacer used to fill DCMD module's channels including orientation, geometry, and flow attack angle.

For spacers that influence the fluid flow:

$$Nu^s = 0.664 * k_{dc} * Re^{0.5} * Pr^{0.33} * \left(\frac{2 * d_{hs}}{l_m}\right)^{0.5} \quad (24)$$

and

$$k_{dc} = 1.654 * \left(\frac{d_f}{t_s}\right)^{-0.039} \varepsilon^{0.75} * \left(sin\left(\frac{\theta}{2}\right)\right)^{0.086} \quad (25)$$

where d_{hs} is hydraulic diameter for spacer filled condition, k_{dc} is spacer geometry geometry correction factor, l_m is the mesh size, H is the spacer thickness, ε is the spacer voidage, and θ the hydrodynamic angle.

For spacers that do not influence the flow direction (one set of filaments is parallel to, and the other is transverse to the flow direction):

$$Nu^s = 0.664 * k_{dc} * Re^{0.5} * Pr^u * \left(\frac{d_{hs}}{l_m}\right)^{0.5} \quad (26)$$

where Re and Pr are calculated by using Equations (19) and (20), respectively, and u is 0.33. The following equation can determine the superficial velocity for a spacer filled channel [27]:

$$u = \frac{V}{W * t * \varepsilon} \quad (27)$$

where ε is the spacer voidage which is defined by the following equation [28]:

$$\varepsilon = 1 - \frac{\pi * d_f^2}{2 * l_m * t_s * sin\theta} \tag{28}$$

d_{hs} is the spacer-filled channel hydraulic diameter and is defined by the following equation [29]:

$$d_{hs} = \frac{4 * \varepsilon}{\left(\frac{2*(W+t)}{W\,t}\right) + (1-\varepsilon) * S_{vsp}} \tag{29}$$

The specific surface of the spacer is defined as

$$S_{vsp} = \frac{4}{d_f} \tag{30}$$

An alternative Nusselt number correlation for the case of a spacer- filled channel has been suggested by Schwager and Robertson [30] and is given by Equation (30):

$$Nu^s = 1.38 * Re^{0.483} * Pr^{0.33} * \left(\frac{d_{hs}}{l_m}\right)^{0.531} \tag{31}$$

Laminar and turbulent condition in channel flow and its influence on heat transfer coefficient can be calculated using Equation (32) suggested by Zhang and Gray [31]

$$Nu^s = k_{dc} * 0.023 * [1 + 6 * \left(\frac{d_{hs}}{L}\right)] Re^{0.8} * Pr^{0.33} \tag{32}$$

where:

$$k_{dc} = 1.923 * \left(\frac{d_f}{t_s}\right)^{-0.168} |sin\theta|^{0.292} \exp\left[-1.601 * |ln\left(\frac{\varepsilon_{sp}}{0.6}\right)^2|\right] \tag{33}$$

Phattaranawik [10] proposed another correlation for space filled case. It can be determined from Equation (34) below:

$$Nu = k_{dc}\left[4.36 + \frac{0.036 * Re * Pr * (D/L)}{1 + 0.0011 * (Re * Pr * (D/L))^{0.8}}\right] \tag{34}$$

3. Experimental Setup

A schematic of the experimental setup for the DCMD module in the Renewable Energy Lab at RMIT University is shown in Figure 5. The solar pond is made of three layers, namely, lower convective zone (LCZ), non-convective zone (NCZ) and upper convective zone (UCZ). The DCMD module contains feed and permeate channels, normally separated by a hydrophobic membrane. For these experiments, a thin plastic sheet (clear polypropylene of 100 µm thickness) replaces the hydrophobic membrane to exclude mass transfer between the feed and permeate channels. Freshwater is circulated through both feed and permeate channels as a heat transfer fluid. A 24 V, self-priming diaphragm pump with a maximum flow rate of 8 L/min is used to pump the water through the system. The feed reservoir tank is filled with 100 L of freshwater, which is pumped to an in-pond heat exchanger in the SGSP to increase the temperature of the feed side fluid. In addition, an evacuated tube solar collector combined with a thermal storage tank (E.T. tank) is used as an auxiliary heat supply. After leaving the SGSP, the freshwater from the feed reservoir was circulated through a heat exchanger in the E.T tank before being fed into the system and returned to the reservoir. In the case of the permeate side, freshwater is transferred from the permeate tank to the top layer of the SGSP to dissipate the heat gained from the feed side fluid. After that, the cooled freshwater passes through the permeate channel in the DCMD module and is then returned to the permeate tank. The 3D structural arrangement of the DCMD

module is presented in Figure 6 and shows the channel gaps, spacers, and membrane sheet.

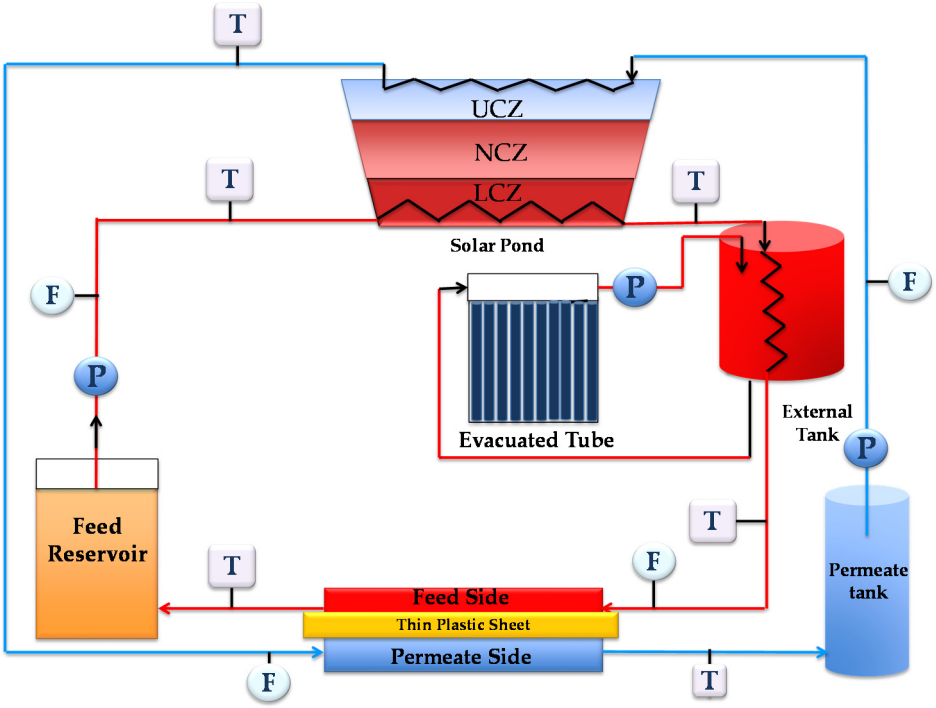


Figure 5. Schematic configuration of the sustainable experimental system using a thin plastic sheet.

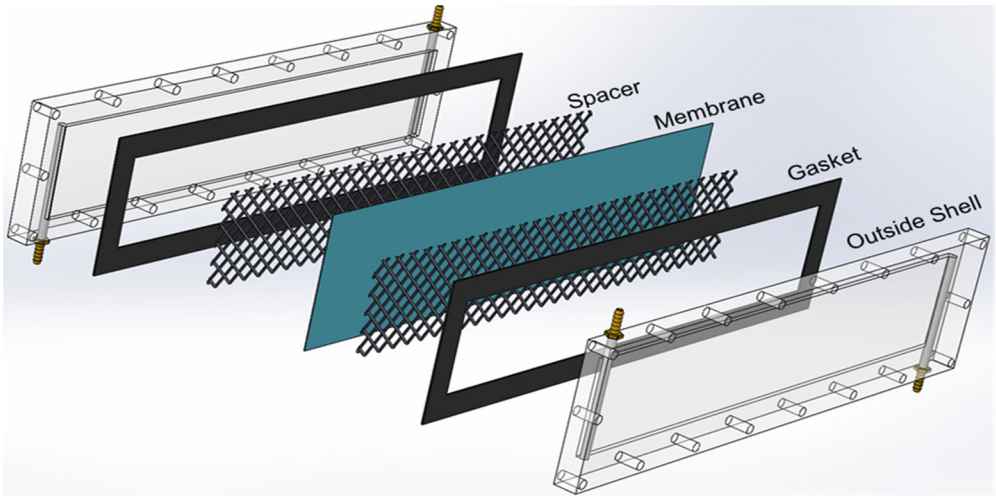


Figure 6. The 3D structural arrangement of the DCMD module.

There are two loops in the proposed system: feed loop and permeate loop. Feed loops experience loss of mass and energy while permeate loops gain mass and energy. Applying energy balance to the feed loop which is connected to the solar pond LCZ and external heater, we can estimate the feed water supply temperature to the feed channel as

$$T_{out_f} = T_{in_f} + \left[\frac{m_{SGSP_LCZ} \times c_{lcz\ water}}{\dot{m}_f \times c_{feed}} \times \frac{\Delta T_{lcz}}{\Delta t}\right] + \left[\frac{\dot{Q}_{heater}}{\dot{m}_f \times c_{feed}}\right] \quad (35)$$

Here, T_{out_f} is the feed water temperatue after it is heated in LCZ and external heater. The mass flow rate of the feed $\dot{m}_f$ is constant while it is getting heated in solar pond and external heater. The specific heat capacity of the feed water and the saline water of LCZ is shown as c_{feed} and $c_{lcz\ water}$, respectively. On the left hand side, the second term in the

square brackets represents the temperature rise of feed water in the solar pond and the third term represent temperature rise in the external heater. In the second square bracket, the mass of the water in solar pond LCZ is given as m_{SGSP_LCZ}, while the ΔT_{lcz} represents change in the temperature of the solar pond LCZ in Δt time step. The time step is relative to the time rate that is used for mass flow rate. The mass and energy balance in the feed channel can be written as

$$\dot{m}_f \times c_{feed} \times T_{in_f_ch} = \left(\dot{m}_f - \dot{m}_{p'}\right) \times c_{feed} \times T_{out_f_ch} + \dot{Q}_{cond} + \dot{m}_{p'} \times h_{fg@T_{f_avg}} \quad (36)$$

Here, the term $\dot{m}_{p'}$ represents the rate of mass transfer that happens from the feed to the permeate side. The temperature of the feed inlet is estimated from Equation (35) and is given as $T_{in_f_ch}$. The change in the mass of the feed due to vapor transport to permeate side is given as $\left(\dot{m}_f - \dot{m}_{p'}\right)$, while the heat transfer through the solid parts of the membrane is given as $\dot{Q}_{cond}$. The mass and energy balance in the permeate channel can be written as,

$$\dot{m}_p \times c_{permeate} \times T_{out_p} = \left(\dot{m}_p + \dot{m}_{p'}\right) \times c_{permeate} \times T_{in_p} + \dot{Q}_{cond} + \dot{m}_{p'} \times h_{fg@T_{p_avg}} \quad (37)$$

Here, the term $\dot{m}_p$ represents the mass flow rate of cold permeate that is coming into the permeate channel. The permeate inlet and outlet temperatures are given as T_{out_p} and T_{in_p}. The mass of the fresh permeate that is added to the permeate flow is recovered as an overflow from the permeate tank. The warm permeate is cooled in the solar pond UCZ heat exchanger and, if needed, in an external cooler. Applying energy balance, we can estimate the temperature of the permeate after the cooling T_{out_p1} as

$$T_{out_p1} = T_{in_p} - \frac{m_{SGSP_UCZ} \times c_{Ucz\ water}}{\dot{m}_p \times c_{permeate}} \times \frac{\Delta T_{ucz}}{\Delta t} + \frac{\dot{Q}_{cooler}}{\dot{m}_p \times c_{permeate}} \quad (38)$$

4. Result and Discussion

The following sections cover the experimental results and discussion of the heat transfer within the DCMD module for both empty channel and spacer filled channel conditions. The experimental results are compared with theoretical Nusselt number correlations to determine the most suitable of these to use for further numerical modelling.

4.1. DCMD Heat Transfer with Empty Channels

In the case of empty channels, the experiment ran with the same setup conditions shown in Figure 7 with two different flow rates. First, a counter flow arrangement uses 3 L/m on both feed and permeate sides. Then, it uses 5 L/m in both channels, also with counter flow. Figure 7 shows the overall heat transfer coefficient calculated from the experimental results for the two different flow rates. The average overall heat transfer coefficient for the 3 L/m tests was 593 W/m^2·°C, and for 5 L/m, it was 724 W/m^2·°C. The experimental results show that the overall heat transfer coefficient increases by approximately 18% at steady state when the flow rate increases from 3 to 5 L/min. In Figures 8 and 9, the feed side outlet temperature (T_{f_out}) is lower than the inlet temperature (T_{f_in}) because of the occurrence of heat transfer to the permeate side. Correspondingly, the outlet temperature of the permeate side (T_{p_out}) increases due to heat transfer through the plastic sheet.

The Reynolds numbers for the two experimental conditions were calculated using Equation (19). They suggested that the flow regime was laminar in both cases. The theoretical Nusselt numbers from heat transfer correlations summarized in Table 1 were calculated for the experimental flow rate conditions presented in Figures 10 and 11. The correlation given by Equation (12) was the most appropriate correlation with a deviation of 10% between the theoretical and the experimental overall heat transfer coefficients.

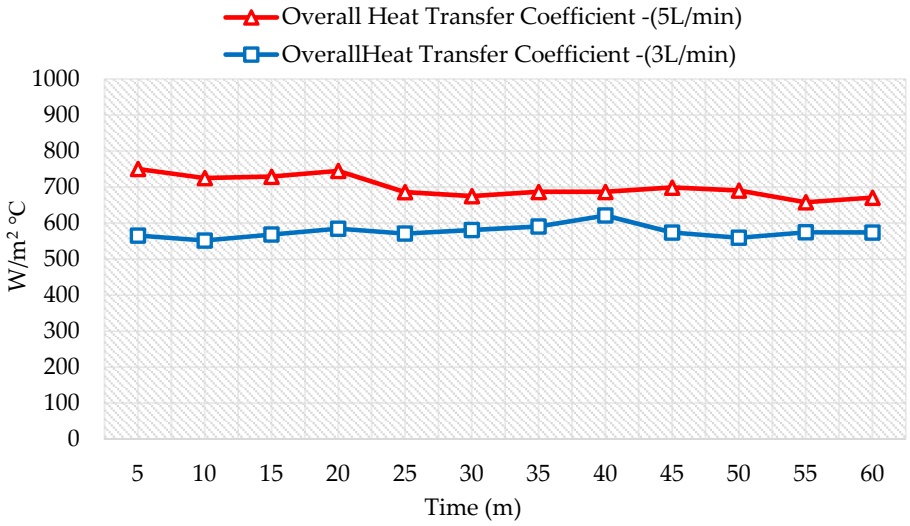


Figure 7. The overall heat transfer coefficient experimentally with different flow rates for the empty channels.

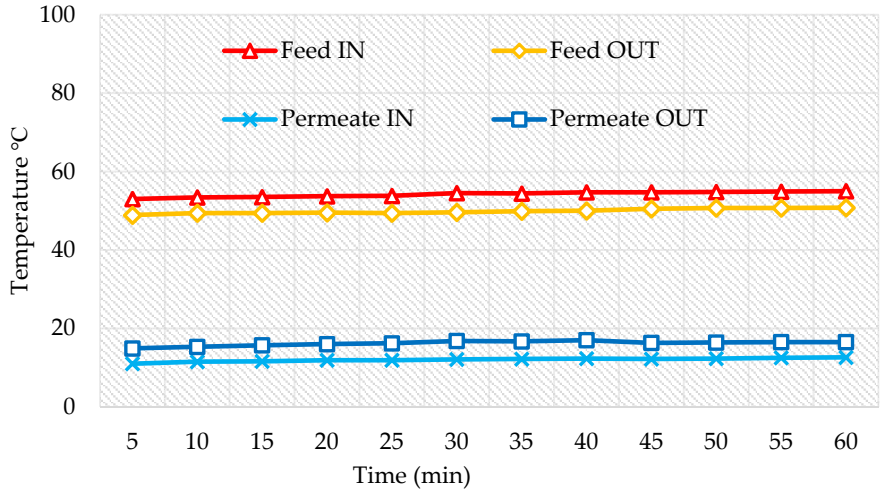


Figure 8. Feed and permeate temperature in case of the empty channel by using 3 L/min.

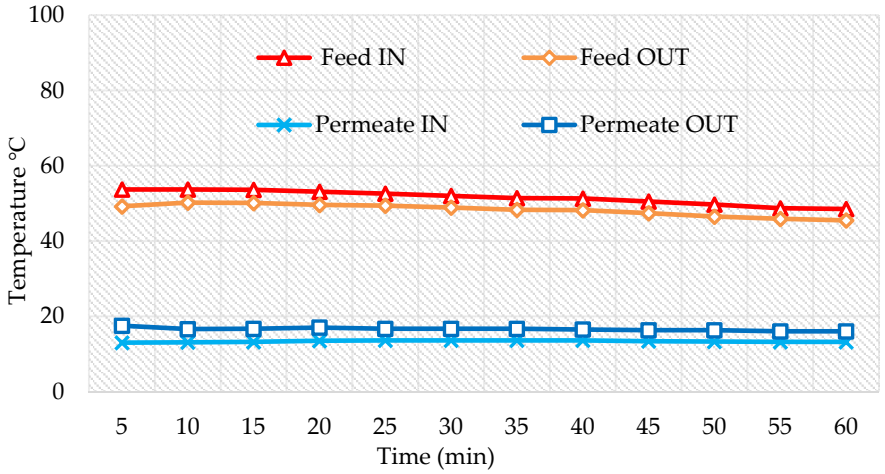


Figure 9. Feed and permeate temperature in case of the empty channel by using 5 L/min.

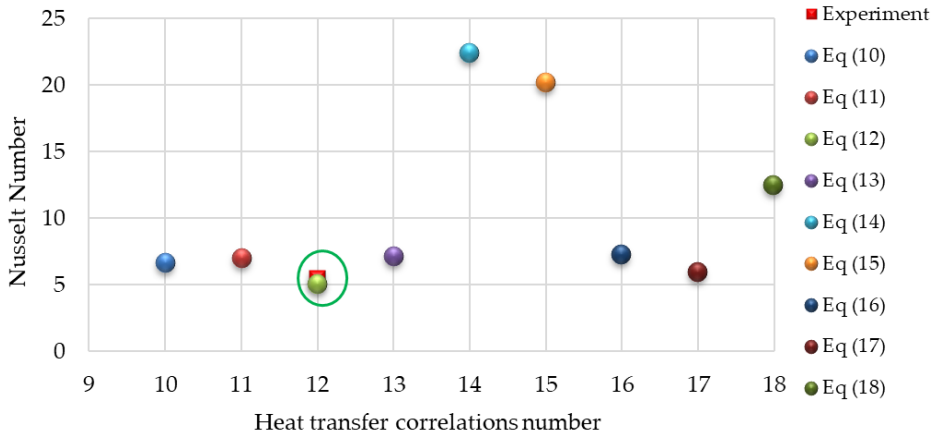


Figure 10. Correlation for empty channel (flow rate = 3 L/m).

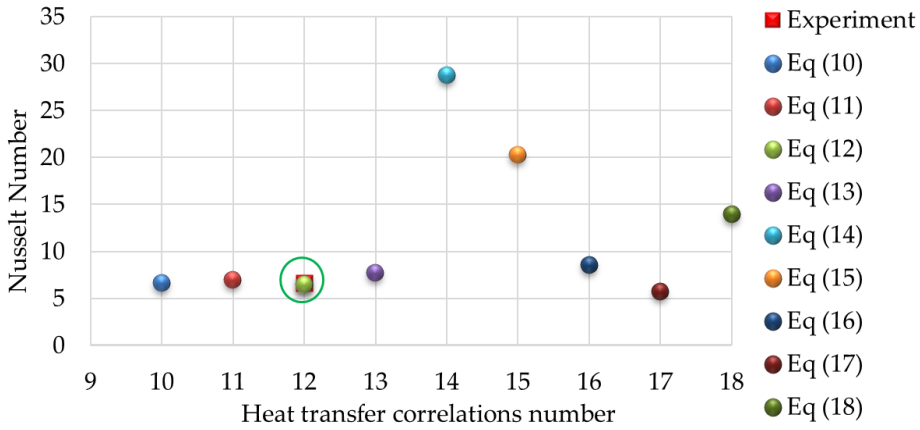


Figure 11. Correlation for empty channel (flow rate = 5 L/m).

4.2. DCMD Spacer-Filled Condition

This system conducted the experiments on the same large-scale DCMD module used for the empty channel experiments with the two different spacer geometries shown in Figure 12 and Table 2. Figure 12(1) shows thinner mesh whereas Figure 12(2) shows thicker mesh.

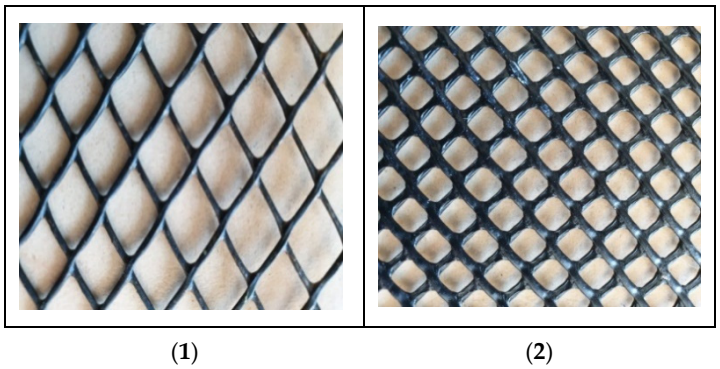


Figure 12. Non-woven plastic spacers (**1**) thin spacer, (**2**) thick spacer.

Similar to the empty, spacer-filled channel, these experiments investigated the conductive heat transfer with each spacer geometry using two flow rates: 3 L/min and then 5 L/min. It can be seen in Figures 13 and 14 that the overall heat transfer coefficient in the case of the spacer-filled channels is higher in the case of empty channels for both 3 and 5 L/min. Comparing just the heat transfer coefficients obtained with each of the two kinds

of spacer, it can be seen that the thicker (2 mm) spacer produces a higher heat transfer coefficient. The average values for overall heat transfer in the case of the spacer-filled channel with a 1.5 mm thick spacer and flow rates of 3 and 5 L/min, were 949 W/m^2·°C and 1379 W/m^2·°C, respectively. Furthermore, the average overall heat transfers for a spacer-filled channel with a 2 mm thick spacer and flow rates of 3 L/m and 5 L/m were 1030 W/m^2·°C and 1465 W/m^2·°C, respectively.

Table 2. Characteristics of spacers.

No.	Spacer	Material	Length (m)	Width (m)	Thickness (m)	Filament size, d_f, (m)	Angle, θ, (°)	Mesh Size, l_m, (m)	Porosity (%)
1	Non-woven	Plastic	0.69	0.1339	0.0015	0.0008	66.5	0.0075	90
2	Non-woven	Plastic	0.69	0.1339	0.0020	0.00156	90	0.0044	57

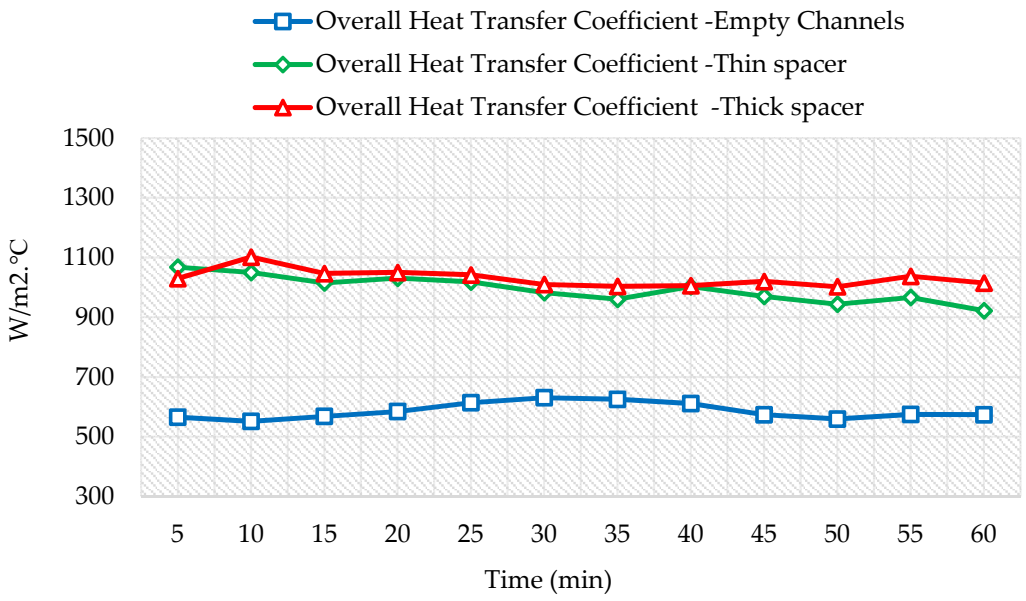


Figure 13. Heat transfer in the empty and spacer-filled channels by using 3 L/min.

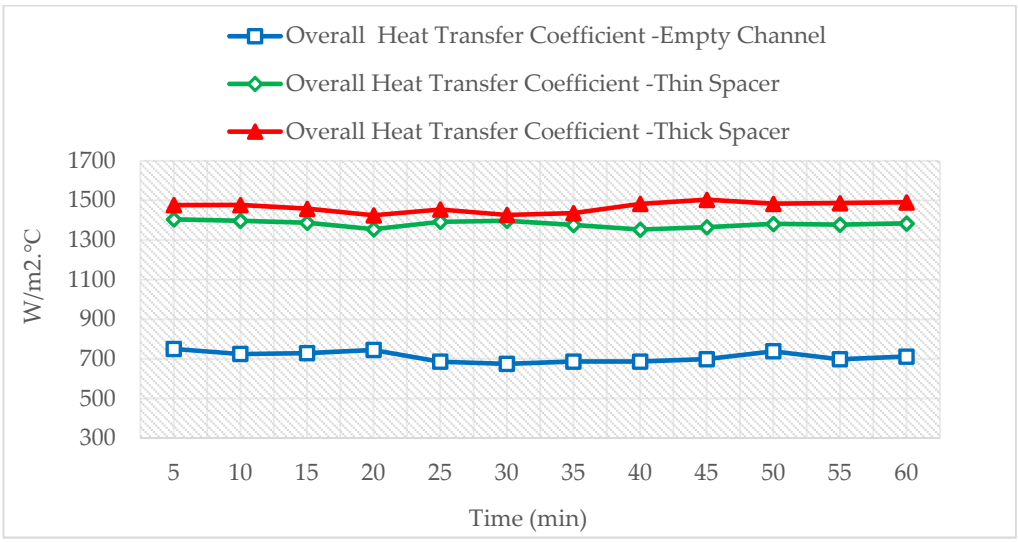


Figure 14. Heat transfer in the empty and spacer-filled channels by using 5 L/min.

It is essential to mention that the DCMD channel thickness was fixed, while the thickness of the two spacers was different. This allowed the thin spacer to float between the

plastic sheet (membrane) and the wall of the DCMD module. The DCMD channel thickness was 2.8 mm, whereas the thin spacer thickness was only 1.5 mm. Therefore, around 46% of the channel was free. As a result, the thin spacer could have effectively created a thinner 'empty channel', which might have influenced the mechanism underlying the increase in the overall heat transfer coefficient observed for the thin spacer compared to the thick spacer. Thicker spacers have also been applied in later experiments, where the spacer filled the channel completely. The thicker space has been observed to produce a slightly better heat transfer performance compared to the thinner spacer, but the overall heat transfer results of both thin and think spacer is very close and cannot be used to call any one of the arrangements better than other.

Based on Equation (19), the Reynolds number was lower than 2100 for all of the channel configurations and flow rates investigated. By knowing the Reynolds number, the flow regime can be predicted, with a number between 600 and 2100 indicating a laminar flow. For this experimental investigation, the bulk flow regime could be considered as laminar for both flow rates and spacers used. The addition of the spacer reduces the height of the cavity and increases the aspect ratio, and this increases the number of eddies [32]. These localized eddies break the boundary layer and reduces the temperature polarization. In the present experiments, the membrane surface temperature is not measured, but the addition of spacers has shown to improve heat transfer. Based on this observation, it is better to have channels with high aspect ratio for a MD system.

Many researchers have investigated correlations for different kinds of channels; their findings were applied to find the best agreement with the experimental results presented from Figures 7–14. A summary of all the experimental and theoretical Nusselt numbers is shown in Figures 15–17. Both Phattaranawik and Jiraratananon [33] and Kim and Francis [34] presented heat transfer correlations for a DCMD module with non-woven spacer-filled channels. Using their correlations, Equations (24) and (26) under the current experimental conditions (1.5 mm and 2 mm spacers; and 3 and 5 L/m flow rates) produced Nusselt number values that differed from experimental results by 90%. Correlations are also given by Equations (31) and (32), which overpredicted the Nusselt number values by 55–72% as compared to experimental results.

The smallest deviation was found using Equation (34) for a 1.5 mm thick non-woven spacer. For both flow rates, the deviation was 10–20%. However, the deviation using the same equation for 2 mm thick spacer-filled channels was greater at 42–55%. Therefore, Equation (34) produces the most appropriate heat transfer correlation among all the equations compared above. Nonetheless, the results from this correlation are still not satisfactory for all cases.

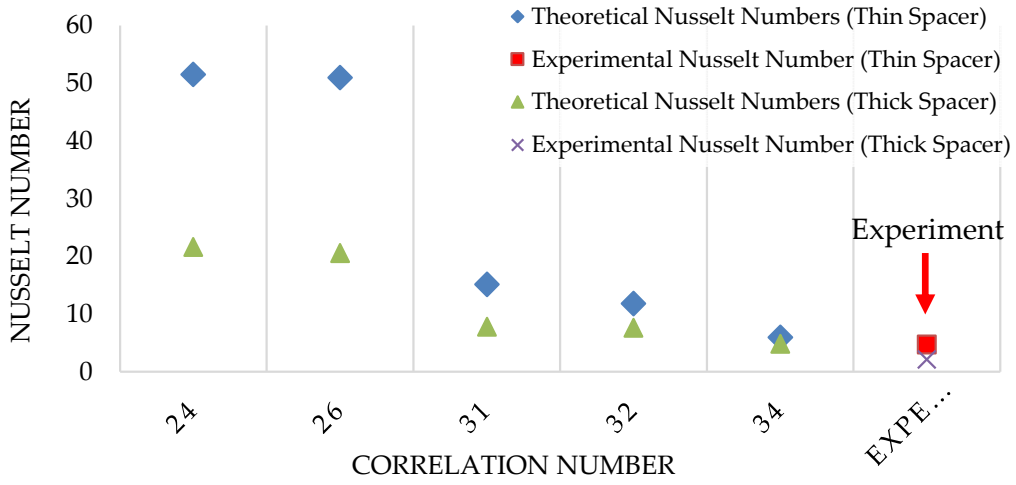


Figure 15. Correlations for spacer-filled channels with flow rate (3 L/min).

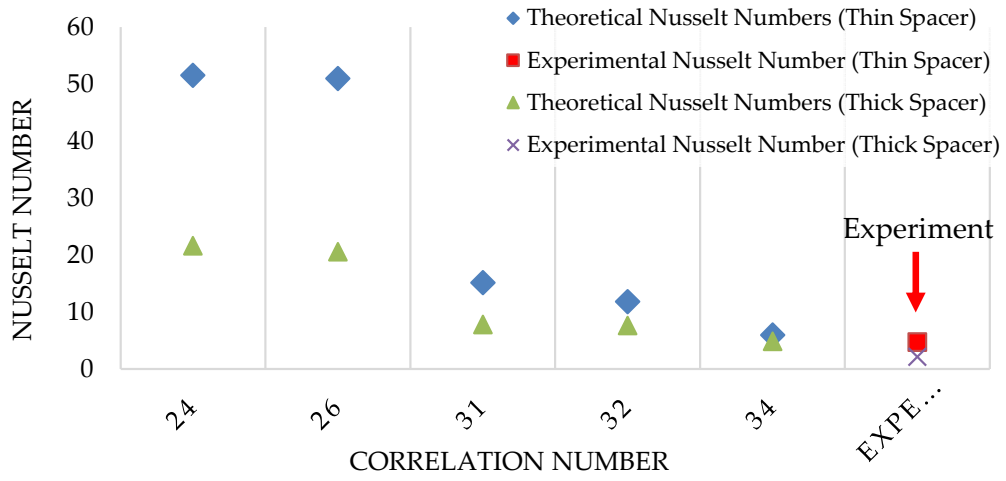


Figure 16. Correlations for spacer-filled channels with flow rate (5 L/min).

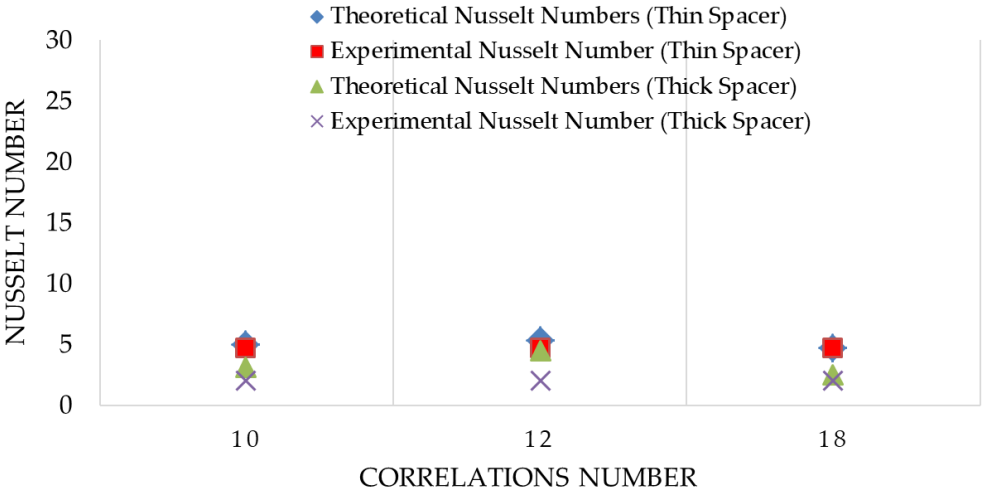


Figure 17. Laminar flow correlation for spacer-filled channels with flow rate (3 L/min).

As discussed above, most of the heat transfer correlations for spacer-filled channels that are recommended for localized turbulence (eddy flow) do not have a good fit with the experimental results from the DCMD module used for this work. Hence, it was decided to estimate the bulk flow conditions based on bulk Reynolds number. Based on the bulk Reynolds number for the experimental results used in this research, the flow regime is identified as laminar, so it was decided to compare the experimental results of the spacer filled channel with the correlations for empty channels (Table 1). For the 1.5 mm spacer, the most appropriate Nusselt number value was achieved using Equations (10) and (12), with a deviation ranging between 5% and 10%. However, considering 1.5 and 2 mm spacers, the heat transfer correlation for laminar flow given by Equation (18) resulted in the smallest deviation between theoretical and experimental results, at less than 15% for all spacer geometries and flow rates tested, as can be seen in Figure 17.

5. Conclusions

The heat transfer within a DCMD module separated by a thin plastic sheet instead of a hydrophobic membrane was analyzed to investigate the applicability of theoretical heat transfer correlations in two cases: empty channels and spacer-filled channels. For empty channels with flow rates of 3 and 5 L/min, the best correlation was provided by Equation (12). The results obtained using this correlation showed a deviation of less than 10% from the experimental results.

The spacer-filled channel cases investigation included two spacer thicknesses (1.5 and 2 mm) and flow rates of 3 and 5 L/min. Other heat transfer correlations for spacer-filled channels were applied, but the lowest deviation between experimental and theoretical results for these correlations was 42%. The experimental results for spacer-filled channels were also compared with the correlations for empty channels. It was found that the correlation given by Equation (18) had the lowest deviation, of less than 15%, for all spacer geometries and flow rates. As a result, the primary benefit of the outcomes of this study comes from identification of the best Nusselt number correlation for use in modelling heat transfer in DCMD systems, assuming similar channel geometries, flow rates and spacer geometries.

The other major outcome based on the experimental results is that including a mesh spacer material in the feed and permeate channels significantly increases the aspect ratio of the channel encouraging eddy flow conditions. This helps with the reduction in the temperature polarization. It should be noted that both 1.5 mm and 2 mm thick spacers resulted in similar improvements (for a 2.8 mm thick channel), with the thicker spacer giving slightly higher heat transfer. However, given the looseness of the fit within the channel for the 1.5 mm spacer, it could not be determined whether these improvements were the result of the same or different underlying mechanisms, so this is recommended as an area for future research.

Author Contributions: Conceptualization, H.F., A.A. and A.D.; data curation, H.F.; formal analysis, H.F. and R.K.; investigation, H.F.; methodology, H.F., M.B. and Q.L.V.; writing—original draft, H.F. and A.D.; supervision, A.A. and A.D., writing—review and editing, H.F., M.B., Q.L.V., O.T., R.K., A.A. and A.D. All authors have read and agreed to the published version of the manuscript.

Funding: This research received no external funding.

Data Availability Statement: The data is an experimental outcome and has been stored with the first author. Data will be made available on request by sending email to hzfaqeha@uqu.edu.sa.

Acknowledgments: Contributors are the coauthors of the manuscript.

Conflicts of Interest: The authors declare no conflict of interest.

Nomenclature

The following abbreviations are used in this manuscript:

A_m	The membrane's active surface area (m^2)
C_p	Specific heat capacity (J/kg·K)
D	Hydraulic diameter (m)
d_f	Filament size (m)
d_{hs}	Hydraulic diameter or the spacer-filled (m)
H	Spacer thickness (m)
h_f	Heat transfer coefficient at feed side ($W/m^2 \cdot °C$).
h_p	Heat transfer coefficient at permeate side ($W/m^2 \cdot °C$)
h_{fg}	Enthalpy of vaporization for water (J/kg)
k	Thermal conductivity ($W/m^2 \cdot °C$).
k_{dc}	Spacer geometry correction factor
l_m	Mesh size of spacer (m)
$\dot{m}$	Flow rate (kg/s)
Nu	Nusselt number
P_r	Prandtl number.
$\dot{Q}_f$	Heat transfer by convection at feed side (W)
$\dot{Q}_p$	Heat transfer by convection at permeate side (W)
$\dot{Q}_{cond}$	Heat transfer by conduction through the membrane (W)
R_e	Reynolds number.
T_f	Average bulk temperature of the feed stream (°C)
T_p	Average bulk temperature of the permeate stream (°C)

$T_{sheet,f}$	Feed side sheet surface temperature (°C)
$T_{sheet,p}$	Permeate side sheet surface temperature (°C)
ΔT_{LMTD}	Log mean temperature difference (°C)
U	The overall heat transfer coefficient (W/m^2·°C)
u	velocity (m/s)
ρ	Water density (kg/m^3)
δ	Membrane thickness (m)
θ	Hydrodynamic angle
ε	Spacer void
l_m	Mesh size of spacer (m)

References

1. Irannezhad, M.; Ahmadi, B.; Liu, J.; Chen, D.; Matthews, J.H. Global water security: A shining star in the dark sky of achieving the sustainable development goals. *Sustain. Horiz.* **2021**, *1*, 100005. [CrossRef]
2. Davis, A.C.; Arnocky, S.; Stroink, M. The problem of overpopulation: Proenvironmental concerns and behavior predict reproductive attitudes. *Ecopsychology* **2019**, *11*, 92–100. [CrossRef]
3. Membrane Distillation. Available online: https://emis.vito.be/en/bat/tools-overview/sheets/membrane-distillation (accessed on 15 October 2022).
4. El-Bourawi, M.S.; Ding, Z.; Ma, R.; Khayet, M. A framework for better understanding membrane distillation separation process. *J. Membr. Sci.* **2006**, *285*, 4–29. [CrossRef]
5. Alves, V.D.; Coelhoso, I. Orange juice concentration by osmotic evaporation and membrane distillation: A comparative study. *J. Food Eng.* **2006**, *74*, 125–133. [CrossRef]
6. Calabro, V.; Jiao, B.L.; Drioli, E. Theoretical and Experimental Study on Membrane Distillation in the Concentration of Orange Juice. *Ind. Eng. Chem. Res.* **1994**, *33*, 1803–1808. [CrossRef]
7. Martínez-Díez, L.; Vázquez-González, M.; Florido-Díaz, F. Study of membrane distillation using channel spacers. *J. Membr. Sci.* **1998**, *144*, 45–56. [CrossRef]
8. Taamneh, Y.; Bataineh, K. Improving the performance of direct contact membrane distillation utilizing spacer-filled channel. *Desalination* **2017**, *408*, 25–35. [CrossRef]
9. Phattaranawik, J.; Jiraratananon, R.; Fane, A.; Halim, C. Mass flux enhancement using spacer filled channels in direct contact membrane distillation. *J. Membr. Sci.* **2001**, *187*, 193–201. [CrossRef]
10. Phattaranawik, J.; Jiraratananon, R.; Fane, A. Effects of net-type spacers on heat and mass transfer in direct contact membrane distillation and comparison with ultrafiltration studies. *J. Membr. Sci.* **2003**, *217*, 193–206. [CrossRef]
11. Yun, Y.; Wang, J.; Ma, R.; Fane, A.G. Effects of channel spacers on direct contact membrane distillation. *Desalination Water Treat.* **2011**, *34*, 63–69. [CrossRef]
12. Taamneh, Y. Heat and fluid flow through a spacer-filled channel in a membrane module. *Heat Transf. Res.* **2017**, *48*, 1567–1580. [CrossRef]
13. Chang, H.; Hsu, J.-A.; Chang, C.-L.; Ho, C.-D. CFD Study of Heat Transfer Enhanced Membrane Distillation Using Spacer-Filled Channels. *Energy Procedia* **2015**, *75*, 3213–3219. [CrossRef]
14. Gong, B.; Yang, H.; Wu, S.; Xiong, G.; Yan, J.; Cen, K.; Bo, Z.; Ostrikov, K. Graphene Array-Based Anti-fouling Solar Vapour Gap Membrane Distillation with High Energy Efficiency. *Nano-Micro Lett.* **2019**, *11*, 1–14. [CrossRef] [PubMed]
15. Ve, L.Q.; Rahaoui, K.; Bawahab, M.; Faqeha, H.; Date, A.; Akbarzadeh, A.; Cuong, D.M.; Nguyen, L.Q. Experimental Investigation of Heat Transfer Correlation for Direct Contact Membrane Distillation in Laminar Flow. *J. Heat Transf.* **2020**, *142*, 12001. [CrossRef]
16. Schofield, R.; Fane, A.; Fell, C. Heat and mass transfer in membrane distillation. *J. Membr. Sci.* **1987**, *33*, 299–313. [CrossRef]
17. Laganà, F.; Barbieri, G.; Drioli, E. Direct contact membrane distillation: Modelling and concentration experiments. *J. Membr. Sci.* **2000**, *166*, 1–11. [CrossRef]
18. Qtaishat, M.; Matsuura, T.; Kruczek, B.; Khayet, M. Heat and mass transfer analysis in direct contact membrane distillation. *Desalination* **2008**, *219*, 272–292. [CrossRef]
19. Franken, A.; Nolten, J.; Mulder, M.; Bargeman, D.; Smolders, C. Wetting criteria for the applicability of membrane distillation. *J. Membr. Sci.* **1987**, *33*, 315–328. [CrossRef]
20. Tijing, L.D.; Choi, J.S.; Lee, S.; Kim, S.H.; Shon, H.K. Recent progress of membrane distillation using electrospun nanofibrous membrane. *J. Membr. Sci.* **2014**, *453*, 435–462. [CrossRef]
21. Gryta, M.; Tomaszewska, M.J.J. Heat transport in the membrane distillation process. *J. Membr. Sci.* **1998**, *144*, 211–222. [CrossRef]
22. Sieder, E.N.; Tate, G.E. Heat Transfer and Pressure Drop of Liquids in Tubes. *Ind. Eng. Chem.* **1936**, *28*, 1429–1435. [CrossRef]
23. Thomas, L. *Heat Transfer*; Prentice-Hall, Inc.: Englewood Cliffs, NJ, USA, 1992.
24. Gryta, M.; Tomaszewska, M.; Morawski, A.W. Membrane distillation with laminar flow. *Sep. Purif. Technol.* **1997**, *11*, 93–101. [CrossRef]
25. Andrjesdóttir, O.; Ong, C.L.; Nabavi, M.; Paredes, S.; Khalil, A.; Michel, B.; Poulikakos, D. An experimentally optimized model for heat and mass transfer in direct contact membrane distillation. *Int. J. Heat Mass Transf.* **2013**, *66*, 855–867. [CrossRef]

26. Chang, H.; Ho, C.-D.; Hsu, J.-A. Analysis of Heat Transfer Coefficients in Direct Contact Membrane Distillation Modules Using CFD Simulation. *J. Appl. Sci. Eng.* **2016**, *19*, 197–206. [CrossRef]
27. Da Costa, A.; Fane, A.; Wiley, D. Spacer characterization and pressure drop modelling in spacer-filled channels for ultrafiltration. *J. Membr. Sci.* **1994**, *87*, 79–98. [CrossRef]
28. Da Costa, A.R. Fluid Flow and Mass Transfer in Spacer-Filled Channels for Ultrafiltration. Ph.D. Thesis, University of New South Wales, Sydney, Australia, 1993.
29. Schock, G.; Miquel, A. Mass transfer and pressure loss in spiral wound modules. *Desalination* **1987**, *64*, 339–352. [CrossRef]
30. Schwager, F.; Robertson, P.; Ibl, N. The use of eddy promoters for the enhancement of mass transport in electrolytic cells. *Electrochim. Acta* **1980**, *25*, 1655–1665. [CrossRef]
31. Zhang, J.; Gray, S.; Li, J.-D. Modelling heat and mass transfers in DCMD using compressible membranes. *J. Membr. Sci.* **2012**, *387–388*, 7–16. [CrossRef]
32. Heaton, C.J. On the appearance of Moffatt eddies in viscous cavity flow as the aspect ratio varies. *Phys. Fluids* **2008**, *20*, 103102. [CrossRef]
33. Phattaranawik, J.; Jiraratananon, R.; Fane, A.G. Heat transport and membrane distillation coefficients in direct contact membrane distillation. *J. Membr. Sci.* **2003**, *212*, 177–193. [CrossRef]
34. Kim, Y.-D.; Francis, L.; Lee, J.-G.; Ham, M.-G.; Ghaffour, N. Effect of non-woven net spacer on a direct contact membrane distillation performance: Experimental and theoretical studies. *J. Membr. Sci.* **2018**, *564*, 193–203. [CrossRef]